Mon. Not. R. Astron. Soc. **000**, 000–000 (0000) Printed 2 February 2008 (MN LATEX style file v2.2)

Sequential and Spontaneous Star Formation Around the Mid-Infrared Halo H II Region KR 140

C. R. Kerton[1⋆], K. Arvidsson[1], Lewis B. G. Knee[2], and C. Brunt[3]
[1]*Department of Physics and Astronomy, Iowa State University, Ames, IA 50011, USA*
[2]*Atacama Large Millimeter Array, Avenida El Golf 40, Piso 18, Las Condes, Santiago, Chile*
[3]*School of Physics, University of Exeter, Stocker Road, Exeter EX4 4QL, UK*

2 February 2008

ABSTRACT
We use 2MASS and *MSX* infrared observations, along with new molecular line (CO) observations, to examine the distribution of young stellar objects (YSOs) in the molecular cloud surrounding the halo H II region KR 140 in order to determine if the ongoing star-formation activity in this region is dominated by sequential star formation within the photodissociation region (PDR) surrounding the H II region. We find that KR 140 has an extensive population of YSOs that have "spontaneously" formed due to processes not related to the expansion of the H II region. Much of the YSO population in the molecular cloud is concentrated along a dense filamentary molecular structure, traced by $C^{18}O$, that has not been erased by the formation of the exciting O star. Some of the previously observed submillimetre clumps surrounding the H II region are shown to be sites of recent intermediate and low-mass star formation while other massive starless clumps clearly associated with the PDR may be the next sites of sequential star formation.

Key words: stars: pre-main-sequence – stars: formation – H II Regions – infrared: stars

1 INTRODUCTION

This study is the fourth in a series of papers exploring the structure of the H II region KR 140 and its associated star-forming activity. In Kerton, Ballantyne, & Martin (1999) VES 735, the O-star powering the H II region was examined. A second paper, Ballantyne, Kerton & Martin (2000), was a multiwavelength study of the structure, energetics, and kinematics of the H II region. Finally, Kerton et al. (2001) presented an analysis of submillimetre (submm hereafter) observations of the region at 450 and 850 μm. The main result of Kerton et al. (2001) was the discovery of numerous submm dust cores located within the molecular gas surrounding the H II region, including a large number of cores that were clearly located at the interface between ionized and molecular gas, a likely location for star-formation induced or "triggered" by the expansion of the H II region (Elmegreen 1998). Two of the more isolated cores were clearly associated with *IRAS* sources, but the low resolution of *IRAS* combined with the extensive diffuse emission of dust associated with the H II region made it impossible to determine if any of the other cores were associated with star-formation activity.

The goal of this study is to determine the distribution of young stellar objects (YSOs) throughout the KR 140 molecular cloud. We focus especially on the embedded stellar content of the submm cores as these are potentially the youngest star-forming regions. We use the spatial distribution of the YSOs relative to the photodissociation region (PDR) surrounding the H II region as a means of gauging the relative importance of spontaneous and sequential, or triggered, star formation in this region. To achieve this we have analyzed a combination of submm data from Kerton et al. (2001) and Moore et al. (2007), 2MASS (2 Micron All Sky Survey) and Midcourse Space Experiment (*MSX*) infrared data, and newly acquired ^{12}CO, ^{13}CO and $C^{18}O$ molecular line data from the Five College Radio Astronomy Observatory (FCRAO). In the next section we review the pertinent parameters of KR 140 and provide information on the new observations of the region. In § 3 and § 4 we first show how 2MASS data can be utilized to identify the YSO population and then examine its spatial distribution. Our results are discussed in § 5 and conclusions are presented in § 6.

2 KR 140: PROPERTIES AND OBSERVATIONS

KR 140 ($l = 133\overset{\circ}{.}425$, $b = +0\overset{\circ}{.}054$; Kallas & Reich 1980) is a 5.7 pc diameter H II region located at a distance of 2.3 ± 0.3 kpc. It is close to, but apparently isolated from, the large W3/W4/W5 star-formation complex. The region is ionized by a single O8.5 V(e) star VES 735. Foreground extinction is $A_V = 5.7 \pm 0.2$ magnitudes toward VES 735 and ranges between $A_V \sim 6 - 7$ over the H II region. Molecular line observations (^{12}CO J=1−0) indicate that the H II region is associated with a molecular cloud with a mass in the range $10^{3.7}$ – $10^{4.0}$ $M_\odot$. A detailed discussion and

⋆ E-mail: kerton@iastate.edu

Table 1. Spatial correspondence between Kerton et al. (2001) and Moore et al. (2007) submm clumps (KMJB and M07 respectively).

KMJB	M07	KMJB	M07
1	37	11	14
2	···	12	11
3	32	13	8 & 10
4	33	14	5
5	26 & 29	15	···
6	25	16	6
7	24	17	···
8	23	18	4
9	17	19	3
10	···	20	···

derivation of these properties can be found in Kerton et al. (1999) and Ballantyne et al. (2000).

2.1 Submillimetre Observations

For this study we used a combined sample of submm clumps identified in the Kerton et al. (2001) and Moore et al. (2007) 850 μm SCUBA scan-maps of the KR 140 region. There are only minor disagreements between the two samples where they overlap due to the different ways in which structures were identified in the two studies and the correspondence between the two samples is shown in Table 1. In the area covered by our molecular-line observations ($2^{\rm h}18^{\rm m}15^{\rm s} \leqslant \alpha_{2000} \leqslant 2^{\rm h}22^{\rm m}30^{\rm s}$ and $60^\circ54' \leqslant \delta_{2000} \leqslant 61^\circ20'$, see § 2.3) there are a total of 39 submm clumps: KMJB 1 - KMJB 20 from Kerton et al. (2001) and clumps 7, 9, 12-13, 21, 39-40, 42-45 and 47-54 from Moore et al. (2007).

2.2 Mid-Infrared *MSX* Observations

Mid-infrared emission from polycyclic aromatic hydrocarbons (PAHs) can be used to detect the PDRs that arise at the interface between ionized gas in an H II region and surrounding molecular material (Giard et al. 1994). We obtained *MSX* Band A ($\lambda_o = 8.3$ μm, $\lambda = 7-11$ μm) images of KR 140 with $20''$ resolution taken as part of the *MSX* Galactic Plane Survey (Price et al. 2001). The Band A emission is dominated by intense line emission from PAHs caused by various C−C stretching and C−H bending modes. An up-to-date listing of the numerous PAH features in the mid-infrared can be found in Draine & Li (2007).

The distinctive mid-infrared morphology exhibited by KR 140 (see Fig. 1) and in other similar H II regions (e.g. Cohen & Green 2001; Deharveng et al. 2003) arises from changes in the relative balance between ultraviolet (UV) photons which preferentially destroy PAHs and those which excite their emission. Deep within the H II region, hard UV radiation destroys PAHs and are themselves destroyed. Outside the PAH-free zone, the remaining UV photons move into the surrounding PDR and excite PAH emission in a layer around the H II region. This layer is relatively thin because UV fluxes continue to drop through the PDR, resulting in a drop in PAH emission. The overall result is a striking ring-like or "halo" morphology. In Fig. 1 we also show the location of the submm clumps discussed in § 2.1: the correspondence between the location of some of the cores and the interface region traced by the mid-infrared emission is evident.

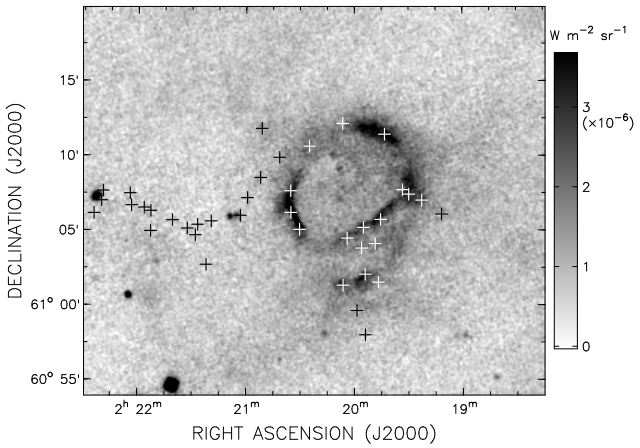

Figure 1. *MSX* Band A (8.3 μm) image of the KR 140 region. Note the distinctive halo morphology of the PDR. White crosses indicate the positions of submm clumps apparently associated with the PDR and black crosses indicate the submm clumps found away from the PDR.

2.3 Molecular Line Observations

We obtained new molecular line observations of KR 140 in order to determine the full spatial extent of the surrounding molecular cloud and to identify any high column density regions. Maps, covering a $0.^\circ8$ square region around KR 140, were obtained in the J=1−0 transition of ^{12}CO (115.3 GHz), ^{13}CO (110.2 GHz) and C^{18}O (109.8 GHz) using the SEQUOIA array on the 14 m FCRAO millimetre-wave telescope (Erickson et al. 1999). The resulting data cubes have a spatial resolution of $\sim 45''$ ($20''$ pixel grid) and a velocity resolution of 0.065 km s^{-1}. Integrated intensity (zeroth moment) ^{12}CO and ^{13}CO maps of emission between $-54 < {\rm V_{LSR}} < -44$ km s^{-1} are shown in Fig. 2. Contours of integrated intensity C^{18}O emission are also shown on each map highlighting the two main regions of high column density found to the east and west of the H II region.

We find a mass of 8500 ± 1000 M$_\odot$ for the cloud based on the integrated ^{12}CO data. A value of $X = 1.9 \times 10^{20}$ from Strong & Mattox (1996) to convert between integrated intensity (K km s^{-1}) and H_2 column density and using a mean molecular weight of 2.29 to account for the molecular nature of the hydrogen and the presence of He. This estimate is larger than that quoted in Ballantyne et al. (2000) mainly because we are using a larger spatial range to define the associated cloud.

2.4 Near-infrared Data

Photometric (*J*,*H*,$K_{\rm s}$[1]) data on YSOs associated with KR 140 were obtained from the 2MASS All-Sky Point Source Catalog (2MASS PSC hereafter) using the on-line GATOR query tool at the Infrared Science Archive (IRSA). Detailed discussion of the survey and the various data products are available in Skrutskie et al. (2006) and Cutri et al. (2003). Here we note that the overall quality of each 2MASS photometric measurement is indicated by a photometric quality flag ("ph_qual") in the 2MASS PSC. Valid measurements are indicated by a ph_qual value of A, B, C, or D for each filter with the signal-to-noise of the detection decreasing as one moves from ph_qual = A through ph_qual = D. Non-detection in a filter is

[1] In this study we use $K_{\rm s}$ and *K* band photometry interchangeably

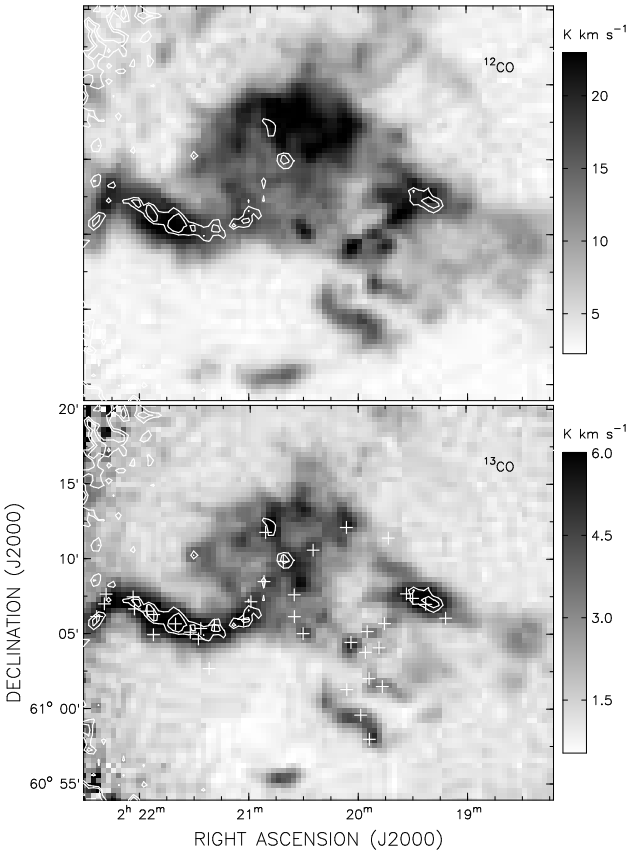

Figure 2. Integrated ^{12}CO (top) and ^{13}CO (bottom) maps of the KR 140 molecular cloud. Contours in both panels show integrated C^{18}O emission at the 1.2 and 1.4 K km s^{-1} levels. White crosses in the lower panel indicate the positions of all detected submm clumps.

typically indicated by ph_qual = U, in which case an upper brightness limit is given.

3 USING 2MASS TO DEFINE THE YSO POPULATION

3.1 *JHK* Colour-Colour and Colour-Magnitude Diagrams

Since we know the distance to KR 140 and the amount of foreground extinction, our approach is to scale observations of different types of YSOs in local star-forming regions to the distance of KR 140, including the effect of foreground extinction, thus defining regions on the *JHK* colour-colour (CC) and colour-magnitude (CM) diagrams where we would expect to find YSOs associated with the KR 140 molecular cloud.

In Fig. 3 we have plotted near-infrared colours of T Tauri stars (approximately solar-mass YSOs with optically thick disks of circumstellar material) from the Kenyon & Hartmann (1995) study of the Taurus-Auriga region (distance $\sim$ 140 pc). Intermediate-mass YSO colours are illustrated using 2MASS photometry for a subset of the Thé, de Winter, & Pérez (1994) catalogue of Herbig Ae and Be stars (HAeBe) that have distance estimates from Finkenzeller & Mundt (1984). One sees that the majority of the sample lies outside of the band of reddened stellar photospheres, with a portion of the T Tauri sample being the main exception. The region occupied by our YSO sample agrees nicely with the CC diagrams constructed using an extensive grid of YSO models presented in Robitaille et al. (2006), once the appropriate amount of foreground extinction is applied to the model-based CC diagrams.

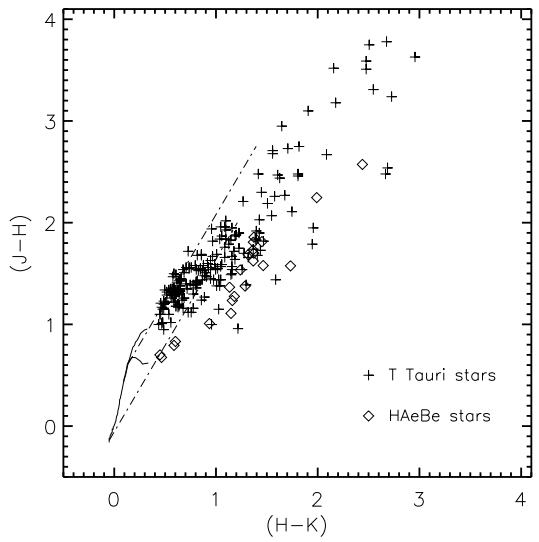

Figure 3. Near-infrared colour-colour diagram. T Tauri and HAeBe data from Kenyon & Hartmann (1995) and Thé et al. (1994) respectively are shown shifted to a distance of 2300 pc and with $A_V = 5.5$ of foreground reddening. The solid lines show the intrinsic colours of main-sequence (V) and giant (III) stars (Koornneef 1983; Bessell & Brett 1988). The dash-dot lines show $A_V = 20$ reddening vectors for a K5 V and O9 V star derived using the infrared extinction law $E(J-H)/E(H-K) = 1.7 \pm 0.4$ from Rieke & Lebofsky (1985).

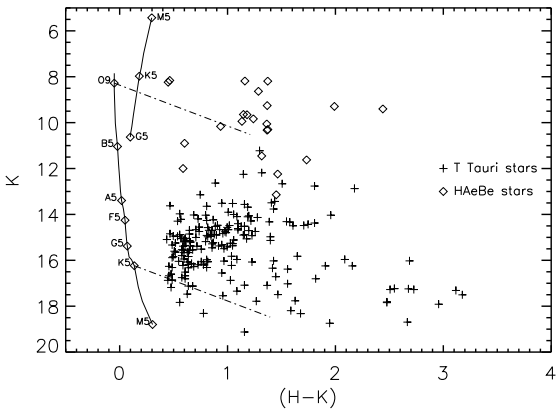

Figure 4. Colour-magnitude diagram for objects at a distance of 2300 pc. Data are the same as in Fig. 3. The main-sequence (V) and giant branch (III) are shown (solid lines) with some representative spectral types labeled. Reddening vectors (dash-dot lines) are drawn for $A_V = 20$ for an O9 V and K5 V star.

The near-infrared CM diagram showing scaled T Tauri and HAeBe data is shown in Fig. 4. The utility of having both the CC and CM diagrams available for data analysis is readily apparent. For example, in the CM diagram the HAeBe sample is clearly distinct from the lower luminosity T Tauri stars. Also, possible confusion between HAeBe stars and giants can be avoided by using the CC diagram, where the two samples are well separated.

Table 2 shows the average magnitude and standard deviation

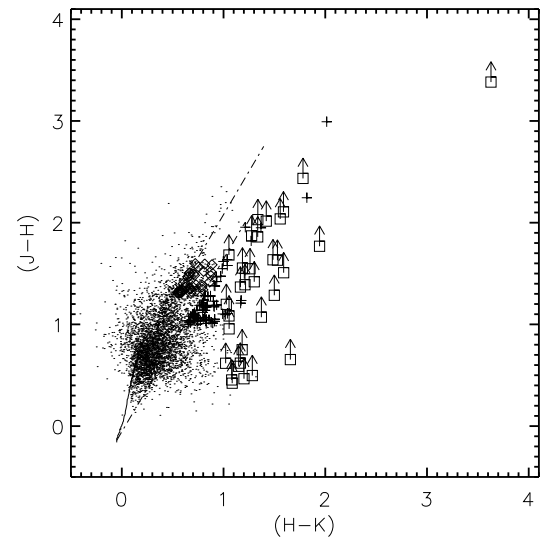

Figure 5. 2MASS Colour-colour diagram. Colours for the 4144 stars with valid *JHK* photometry are plotted (dots) along with colours of the P1 (crosses), P1+ (diamonds), and P2 (squares) YSO samples. The P2 ($J-H$) colours are lower limits (indicated by the arrows). Note, for clarity, error bars are *not* shown.

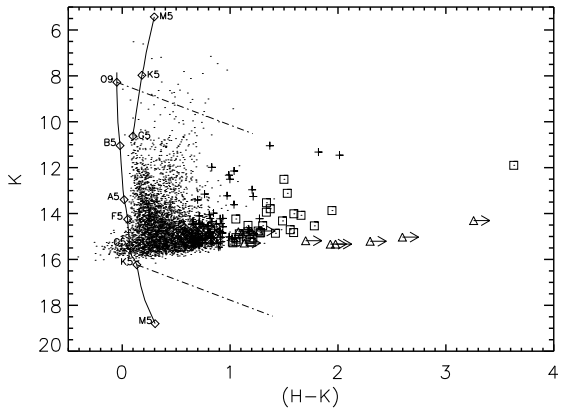

Figure 6. 2MASS Colour-magnitude diagram. As Fig. 5 but also showing the P3 (diamond) YSO sample. The P3 ($H-K$) colours are lower limits (indicated by the arrows).

along with the maximum and minimum magnitude for each of the YSO samples. Also tabulated are the 2MASS limiting magnitudes for a complete sample ("10σ") and for ph_qual = D quality photometry ("D"; see § 2.4). We see that HAeBe stars will be detected in all three bands within the 10σ limits. T Tauri stars will also be detected in all three bands although the sample will be incomplete, missing very heavily embedded sources

3.2 The YSO Population of KR 140

Using the integrated CO maps as a guide we investigated a $0.^{\circ}5 \times 0.^{\circ}4$ region centered on the KR 140 H II region ($2^{\rm h}18^{\rm m}15^{\rm s} \leqslant \alpha_{2000} \leqslant 2^{\rm h}22^{\rm m}30^{\rm s}$ and $60^{\circ}54' \leqslant \delta_{2000} \leqslant 61^{\circ}20'$). The 2MASS PSC was queried using the GATOR software at IRSA. All of the

Table 2. *JHK* magnitudes of YSO samples at 2300 pc.

Sample	Band	Avg.	σ	min	max	$10\sigma^a$	D^b
HAeBe	*J*	12.73	1.8	9.30	16.41	15.8	17.2
	H	11.28	1.5	8.62	14.59	15.1	16.1
	K	10.03	1.4	8.16	13.14	14.3	15.3
T Tauri	*J*	18.21	2.0	13.91	25.73	15.8	17.2
	H	16.50	1.6	12.52	21.36	15.1	16.1
	K	15.44	1.3	11.22	19.12	14.3	15.3

[a] 2MASS completeness limits.
[b] 2MASS ph_qual = D limits for KR 140 region.

catalogue searches and the criteria used to identify YSOs discussed below are summarized in Table 3. Figs. 5 and 6 show both the YSO and non-YSO population of the region for comparison while Fig. 7 shows the spatial location of the YSO sample.

We first searched for all stars with valid photometry (i.e., ph_qual values of A, B, C, or D in all three bands[2]). This search returned 4144 stars from the catalogue. The surface density of stars is fairly uniform across the search area at ~ 4.7 stars /$\Box'$ ($1\sigma = 1.3$). Within this sample of stars we searched for YSOs defined as stars with $(J-H) > 1$ and $(J-H) < 1.7\,(H-K) - 0.075$. The first limit on $(J-H)$ reflects the fact we expect there to be sufficient foreground extinction to push any YSO above the $(J-H) > 1$ line. The second criteria selects stars lying redward of the reddening vector associated with an O6 V star. This search finds 72 stars which we call the P1 sample.

We did an additional search for stars that may be located in the overlap region of T Tauri stars and reddened stellar photospheres. This region is located between $1.3 < (J-H) < 1.6$ and between the two main-sequence reddening vectors. We also required that $K > 14.5$ in order to reduce contamination from giant stars and distant early main-sequence stars. This results in an additional 38 stars, which we call the P1+ sample. We note the conclusions of this paper are not sensitive to whether or not one uses the more conservative selection criteria of the P1 sample or the combined P1 and P1+ sample of 110 stars. We expect that any contamination of the larger sample will arise from distant A and F main-sequence stars as closer, later spectral type stars will tend not to have enough extinction to match the colour criteria.

The KR 140 region was then re-examined for stars with an upper brightness limit at *J* and valid *H* and *K* photometry (ph_qual = [U][A-D][A-D]). This catalogue search returned 133 stars. Possible YSOs were defined using $(H-K) > 1$ and $(J-H) < 1.7\,(H-K) - 0.075$. The latter constraint places the $(J-H)$ lower limit below the reddened stellar photosphere region of the CC diagram. In total 33 stars match these criteria and we identify them as the P2 sample.

Finally we searched the region for stars with only upper brightness limits in *J* and *H* along with valid *K* band photometry (ph_qual = [U][U][A-D]). Of the 37 stars found, 10 of them were defined as possible YSOs by requiring the lower limit of $(H-K) > 1$.

[2] ph_qual MATCHES [A-D][A-D][A-D] in SQL used by GATOR

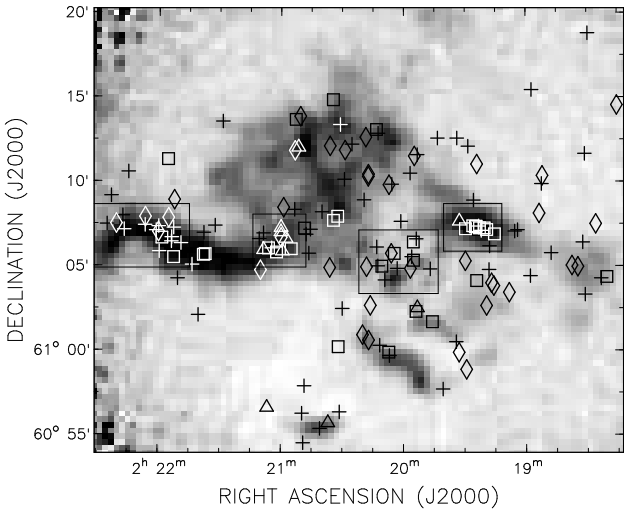

Figure 7. The spatial distribution of the P1 (crosses) P1+ (diamonds), P2 (squares) and P3 (triangles) YSO samples are shown against the integrated ^{13}CO emission associated with KR 140. The boxes show the location of the four concentrations of YSOs discussed in the text, Region A-D, from left to right. White or black symbols are used interchangeably depending on the background level.

Table 3. YSO samples.

Sample	Number	ph_qual values	Colour limits[a]
P1	72	[A-D][A-D][A-D]	$(J-H) > 1$
			$(J-H) < 1.7(H-K)-0.075$
P1+	38	[A-D][A-D][A-D]	$1.3 < (J-H) < 1.6$
			$(J-H) < 1.7(H-K)-0.075$
			$(J-H) < 1.7(H-K)+0.3805$
			$K > 14.5$
P2	33	[U][A-D][A-D]	$(J-H)_L < 1.7(H-K)-0.075$
			$(H-K) > 1.0$
P3	10	[U][U][A-D]	$(H-K)_L > 1.0$

[a] $(J-H)_L$ and $(H-K)_L$ indicate lower limits.

4 THE YSO POPULATION OF THE KR 140 MOLECULAR CLOUD

Using the 2MASS sample defined above, we now explore two questions: 1) What is the association between the YSOs and the submm sources identified by Kerton et al. (2001) and Moore et al. (2007), and 2) What is the overall spatial distribution of the YSOs through the molecular cloud?

4.1 YSOs and Submm Sources

The submm clumps identified by Kerton et al. (2001) have typical diameters of 0.5 pc (10^5 AU), which is about an order of magnitude larger than the 0.05 pc (10^4 AU) size scale typically associated with the smaller core structures within molecular clouds thought to be forming individual stars, for example, the Kirk, Johnstone, & Di Francesco (2006) observations of the Perseus molecular cloud and the Class 0/I YSO models of Robitaille et al. (2006). Thus it is quite possible that a single clump will have multiple sites of star-formation associated with it and that these regions need not correspond with the peak position of the submm emission. We examined our entire YSO sample for positional associations. For the Kerton et al. (2001) sample we used a search radius of $D_{\rm eff}/2$, where $D_{\rm eff}$ is the deconvolved FWHM of a Gaussian fit to an azimuthally-averaged profile of each source. The average search radius was 0.18 pc. Since we do not have size information for the Moore et al. (2007) sample, we used a $20''$ search radius (0.22 pc at 2.3 kpc) for each source in that sample. Table 4 shows the results of this search. Column 1 gives the clump ID number. Columns 2 through 5 contain the 2MASS PSC source number for associated YSOs from the P1, P1+, P2, and P3 samples respectively. Column 7 contains the column density of the submm core expressed in terms of visual extinction, A_V. For the Moore et al. (2007) samples masses were calculated for a distance of 2.3 kpc and a clump temperature of 20 K assuming that all the clumps had a diameter of 0.36 pc. This results in $A_V \sim 10 S_{850}$ where S_{850} is the integrated flux density at 850 μm. All of these A_V estimates are very rough as the column density will vary with the square of the estimated diameter and the temperature enters in through the exponential in the Planck function. Values for the remaining cores were taken from Kerton et al. (2001). Finally, Column 7 denotes if the core is apparently isolated or associated with the PDR. The table includes two submm clumps, 3 and 53m, that have only associated *IRAS* sources and are possible Class 0/I YSOs.

In Fig. 8 and Fig. 9 we plot the CC and CM diagrams showing the YSOs associated with the submm clumps. The CM diagram clearly separates the intermediate-mass YSOs (HAeBe stars) associated with clumps 1, 4 and 19, from the lower luminosity (solar mass or T Tauri) YSOs. The former objects provide an important constraint on the timing of star-formation throughout the molecular cloud as HAeBe stars clear substantial portions of surrounding molecular material on timescales of $\sim 10^6$ years (Fuente et al. 1998).

The T Tauri YSOs found associated with the submm clumps, and those associated with the dense C^{18}O filament (see § 4.2), are also likely tracing star formation on similar time scales. Given that the typical radius for the submm clumps is only 0.25 pc and the velocity dispersion of T Tauri stars is typically 1–2 km s^{-1} (Neuhauser et al. 1998) it will only take the T Tauri star 0.2–0.4 Myr to no longer be associated with the clump as seen by an observer (assuming, for example, that the star is moving at 45° to the line-of-sight). Similarly YSOs associated with the C^{18}O filament have not had enough time to disperse far from their point of origin.

There is growing observational evidence from the analysis of large-scale maps of molecular clouds that star-formation is more likely to occur in high column density regions of molecular clouds where a lower ionization fraction can reduce the efficiency of magnetic support (McKee 1999) and/or turbulent magnetohydrodynamic support (Ruffle et al. 1998). Many studies have found an extinction threshold (A_V^t) where regions with $A_V > A_V^t$ are able to collapse and fragment to form stellar-sized structures; observed values range from $A_V \sim 4$ for Taurus (Onishi et al. 1998), through $A_V \sim 6$ for Perseus (Kirk et al. 2006) to values around $A_V \sim 15$ for Ophiuchus (Johnstone, Di Francesco, & Kirk 2004). The Hatchell et al. (2005) study of Perseus does not show such a clear threshold, but does find an increasing probability of finding cores at increasing levels of A_V. We note that all of these studies refer to the conditions required for core formation and do not consider the YSO content of the core.

In Fig. 10 a histogram shows how the number of clumps with and without associated YSOs varies as a function of A_V. While we do not see an obvious single threshold value it does appear that star-formation is very unlikely to occur in the very low column density clumps. There are 14 clumps with $A_V < 4$, of which 11 (79%)

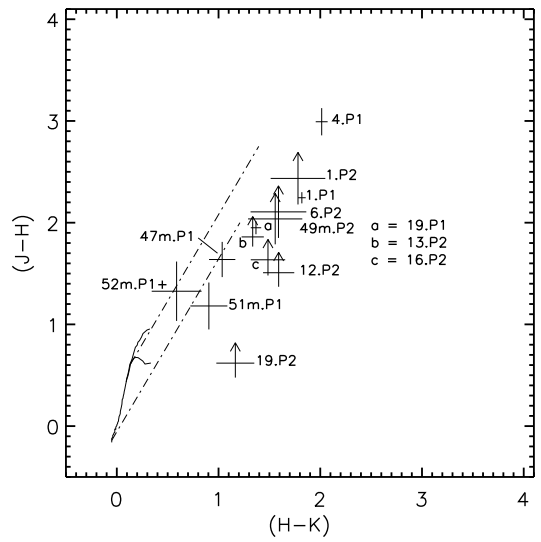

Figure 8. As in Fig. 5 but showing the position of YSOs spatially associated with submm clumps. The size of the symbols indicate the uncertainty in colour. YSOs are identified using the nomenclature from Table 4, e.g., the YSO from the "P2" sample associated with clump 13 is labeled "13.P2". A lower limit to the *(J−H)* colour is indicated by an arrow symbol.

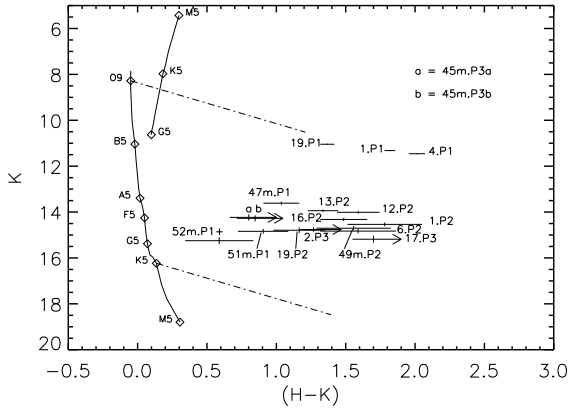

Figure 9. As in Fig. 6 but showing the position of YSOs spatially associated with submm clumps. The size of the symbols indicate the uncertainty in magnitude and colour. YSOs are identified using the nomenclature from Table 4, e.g., the YSO from the "P2" sample associated with clump 13 is labeled "13.P2". A lower limit to the *(H−K)* colour is indicated by an arrow symbol.

do not have associated YSOs and it is unlikely that star formation will occur in these clumps. At the other end of the extinction range all three of the clumps with $A_V > 20$ have YSOs. The remaining 22 clumps with $4 < A_V < 20$ are essentially evenly split, with 10 having associated YSOs and 12 not having YSOs. Based on the studies of other star-forming regions mentioned above we interpret the clumps in this extinction range without YSOs as being *potential* star-formation sites. The lack of detectable YSOs with these clumps could reflect their relative youth, or it may be the case that any YSOs that have formed may be very low mass and thus fall below the 2MASS detection limits even for our P3 sample.

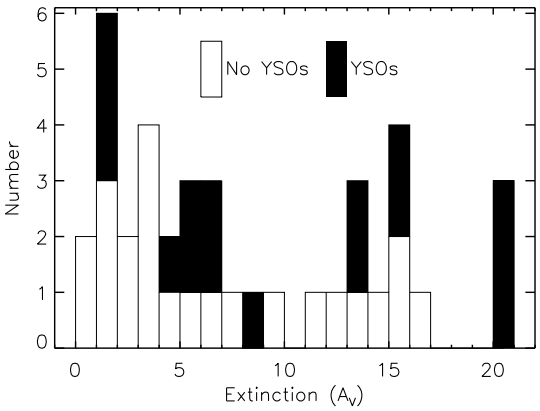

Figure 10. Plot showing the number of clumps with (black) and without (white) YSOs as a function of clump extinction for the combined Kerton et al. (2001) and Moore et al. (2007) sample. For example, there are 5 clumps with $1 \leqslant A_V < 2$ of which 2 have associated YSOs and 3 do not. The rightmost bin includes all clumps with $A_V \geqslant 20$.

4.2 General YSO Spatial Distribution

Visually there appear to be four concentrations of YSOs in the KR 140 molecular cloud (for discussion we will denote these Regions A through D) along with a noticeable lack of YSOs in the northeast portion of the molecular cloud (see Fig. 7). Region A is at the eastern end of the molecular filament near $2^{\rm h}22^{\rm m}$, Region B is associated with submm clump 1 at $2^{\rm h}21^{\rm m}$, Region C is near the central PDR at $2^{\rm h}20^{\rm m}$, and finally Region D is associated with clumps 17, 18 and 19 near $2^{\rm h}19^{\rm m}30^{\rm s}$. To quantify this visual impression we divided the molecular cloud area into $2' \times 2'$ boxes and counted the number of stars falling within each box as a rough measure of the YSO surface density. The average number of YSOs/box is 0.7 ± 1.4 ($\pm 1\sigma$) and boxes near the four regions in question had surface densities of 7, 7, 6 and 11 for A to D respectively. There were no other regions in the molecular cloud with similar $> 3\sigma$ deviations from the average value.

Region A consists of 17 YSOs, four of which are associated with submm clumps. All of the YSOs in this region are T Tauri-like with an average *(H−K)* value of 0.92 ± 0.25. None of the YSOs are coincident with *IRAS* 02186+6033 (MSX6C G133.6890+00.1643), strengthening its identification as a Class 0/I YSO.

The focal point of Region B is the submm clump KMJB 1 which was identified as a Class I YSO (*IRAS* 02174+6052) in Kerton et al. (2001). The higher resolution of the *MSX* and 2MASS data reveal that Clump 1 contains two YSOs, including an intermediate-mass HAeBe which is also a *MSX* point source with a very red mid-infrared spectrum ($F_{8.3} = 0.22$ Jy, $F_{14.65} = 0.73$ Jy). Just to the east of the clump there are two very red YSOs. 2MASS 02210851+6105582 is detected only in one 2MASS band with $K = 14.306$ and a lower limit colour of $(H-K)_L > 3.26$. It is also a bright *MSX* point source (MSX6C G133.5561+00.0919) with an extremely red spectrum ($F_{8.2} = 0.34$ Jy, $F_{14.65} = 1.4$ Jy). The other YSO, 2MASS 02210610+6106043, is detected in both the *H* and *K* bands and has $(H-K) = 3.63$ and $K = 11.899$. Both of these YSOs are probably more highly embedded versions of 1.P1. In addition, just to the west of KMJB 1, there is another highly embedded YSO with $K = 15.208$ and $(H-K)_L > 2.30$. It is quite likely that these objects have formed together as a single grouping of stars.

Table 4. YSOs associated with submm clumps.

	2MASS YSO sample					PDR (P)
Clump ID[a]	P1	P1+	P2	P3	A_V	or Isolated (I)
1	02210449+6106045[b]	···	02210217+6105496	···	5.1	I
2	···	···	···	02205994+6107173	1.6	I
3[c]	···	···	···	···	4.5	I
4	02205329+6108215	···	···	···	15.4	I
6	···	···	02203428+6107425	···	13.1	P
12	···	···	02195506+6105211	···	68.2	P
13	···	···	02195384+6102192	···	1.4	P
16	···	···	02194584+6101426	···	1.1	P
17	···	···	···	02193257+6107399	8.7	P
19	02192184+6107069	···	02192272+6107157	···	21.7	P
45m	···	···	···	02214126+6105457	37.7	I
				02214085+6105439		
47m	02215369+6106275	···	···	···	6.8	I
49m	···	···	02215837+6106405	···	5.4	I
51m	02220660+6107253	···	···	···	6.5	I
52m	···	02222067+61073111	···	···	15.7	I
53m[d]	···	···	···	···	13.4	I

[a] Moore et al. (2007) ID numbers have a trailing m (e.g. 7m), other ID numbers from Kerton et al. (2001)
[b] 2MASS 02210449+6106045 = MSX6C G133.5492+00.0900
[c] *IRAS* 02171+6058
[d] *IRAS* 02186+6033 = MSX6C G133.6890+00.1643

Region C is interesting because of its association with the PDR ridge seen in the *MSX* images. The majority of the stars are found to the northeast of the PDR, while 5 of the remaining 6 stars are found along the PDR with one of the YSOs being coincident with a submm clump. This pattern suggests that star-formation is progressing from northeast to southwest with the submm clumps found along the PDR being the latest round of star formation.

Region D contains the submm clumps 17, 18, and 19. Intermediate-mass and solar-mass YSOs are associated with clump 19 and, just to the north of this clump, there are an additional six T Tauri YSOs. All three of these clumps make up the infrared source *IRAS* 02157+6053 which *MSX* and 2MASS now clearly show is actually a concentration of YSOs combined with extended emission from the PDR.

5 DISCUSSION

5.1 Spontaneous versus Sequential Star Formation

When examining star formation processes within a molecular cloud containing an H II region, a key distinction is between sequential star formation, where the trigger for star formation is directly related to the presence of the H II region (e.g., Deharveng, Zavagno & Caplan 2005), and spontaneous star formation, which occurs with no apparent causal relationship with the H II region. It is well known that for both classical density-bounded H II regions and blister/champagne-flow H II regions, the ionization front (IF) is preceded by a shock front as it propagates into the molecular cloud (Osterbrock 1985; Bedijn & Tenorio-Tagle 1981). Time-dependent models of PDR/IF development around OB stars (Roger & Dewdney 1992; Diaz-Miller, Franco & Shore 1998) show that the IF and PD front merge rapidly, i.e., on time scales less than the main-sequence lifetime of the exciting star, for typical molecular cloud densities. With this in mind it is useful to consider two distinct environments within the molecular cloud; the region beyond the direct influence of the H II region, and the PDR, which is the region directly influenced by the expansion and UV flux of the H II region and which can be clearly traced by PAH emission. A comparison of the YSO population found in each of these regions then gives a measure of the relative importance of sequential and spontaneous star formation within the molecular cloud.

To delineate these two regions we use the 1.5×10^{-6} W m^{-2} sr^{-1} contour in the *MSX* Band A image to (generously) define the extent of the PDR. We find that 42% of the full YSO sample (P1, P1+, P2 and P3) lie within the PDR as defined and 58% lie outside the PDR. The exact percentages will vary somewhat depending on how the PDR is defined. For example, using a more conservative definition for the PDR region (1.75×10^{-6} W m^{-2} sr^{-1}) results in 31% of the YSOs within the PDR and 69% outside the PDR. The percentages, in both cases, are the same for the YSO population both with and without including the P1+ sample. In all cases it is clear that a substantial fraction of the YSO population lies beyond the PDR in this star-forming region and is thus *not* the result of sequential star formation associated with the H II region.

5.2 A Scenario for Star Formation in KR 140

The exciting star of the H II region, VES 735, is about 2 Myr old (Kerton et al. 1999), and kinematic models of the H II region set expansion timescales of 1-2 Myr (Ballantyne et al. 2000). Our observations and analysis of KR 140 are consistent with a molecular cloud undergoing continuous star formation over this period. There is no clear signature of a significant older population of stars seen in the 2MASS photometry of the region (see Figs. 5 and 6). Lower mass YSOs that formed at the same time as VES 735 have had time to disperse through the molecular cloud and may form some of the more spatially distributed population of YSOs seen in our sample.

The expansion of the H II region has swept up material which has subsequently collapsed to form the submm clumps that we ob-

serve in the PDR. At the same time the elongated morphology of the densest portion of the molecular cloud has resulted in ongoing star formation in regions well away from the direct influence of the H II region. As discussed earlier, the association of HAeBe and T Tauri stars with dense regions traced in the submm and $C^{18}O$ support ages of $\lesssim 10^6$ years. The presence of the Class 0/I YSOs, *IRAS* 02171+6058 and *IRAS* 02186+6033 shows there continues to be very recent star formation activity on the timescale of $\sim 10^5$ years (Robitaille et al. 2006).

Finally, many of the massive, apparently starless, submm clumps associated with the PDR may represent the next sites of star formation in the molecular cloud. Deeper images of the region at longer wavelengths would be able to determine if these clumps are starless and test the scenario outlined above by being able to distinguish between different YSO evolutionary stages (Robitaille et al. 2006).

6 CONCLUSIONS

While much of the focus of studies of star formation in and around H II regions is on the interface regions, our study of KR 140 illustrates that spontaneous star formation occurring away from the interface regions in these molecular clouds can be as important as sequential or triggered star formation related to the expansion of the H II region. Our analysis shows that the molecular cloud associated with KR 140 contains an extensive population of YSOs that is not associated with the PDR.

We have also shown that this YSO population is not uniformly distributed though the molecular cloud but is concentrated in four distinct regions. Many of the YSOs are also clearly associated with a filamentary structure within the molecular cloud which is traced by $C^{18}O$ emission. Finally, we see that both low-mass and intermediate-mass YSOs are forming throughout the molecular cloud. Particularly interesting is the region around KMJB 1 (*IRAS* 02174+6052) which contains a tight grouping of a number of embedded intermediate-mass and solar-mass YSOs including the very highly embedded intermediate-mass YSO 2MASS 02210610+6106043.

ACKNOWLEDGMENTS

This research has made extensive use of the NASA/IPAC Infrared Science Archive (IRSA), the Canadian Astronomy Data Centre (CADC), and data from the Two Micron All Sky Survey (2MASS). IRSA is operated by the Jet Propulsion Laboratory, California Institute of Technology, under contract with NASA. 2MASS is a joint project of the University of Massachusetts and the Infrared Processing and Analysis Center/California Institute of Technology, funded by NASA and the NSF. The CADC is operated by the National Research Council of Canada with the support of the Canadian Space Agency. FCRAO was supported by NSF grant AST 0540852. CB is supported by an RCUK Fellowship at the University of Exeter, UK. The authors would like to acknowledge the work done by Caroline Pomerleau in the initial stages of this project supported by the Women in Engineering and Science program of NRC Canada.

REFERENCES

Ballantyne, D.R., Kerton, C.R., Martin, P.G., 2000, ApJ, 539, 283
Bedijn, P.J, Tenorio-Tagle, G., 1981, A&A, 98, 85
Bessell, M.S., Brett, J.M., 1988, PASP, 100, 1134
Cohen, M., Green, A.J., 2001, MNRAS, 325, 531
Cutri, R.M. et al., 2003, Explanatory Supplement to the 2MASS All Sky Data Release (Washington: NASA), http://www.ipac.caltech.edu/2mass/releases/allsky/doc/explsup.html
Diaz-Miller, R.I., Franco, J., Shore, S.N., 1998, ApJ, 501, 192
Deharveng, L., Zavangno, A., Salas, L., Porras, A., Caplan, J., Cruz-Gonzalez, I., 2003, A&A, 399, 1135
Deharveng, L., Zavagno, A., Caplan, J., 2005, A&A, 433, 565
Draine, B.T., Li, A., 2007, ApJ, 657, 810
Elmegreen, B.G., 1998, in Woodward, C.E., Shull, J.M., Thronson Jr., H.A., eds, ASP Conf. Ser., Vol. 148, Origins, Astron. Soc. Pac., San Francisco, p. 150
Erickson, N.R., Grosslein, R.M., Erickson, R.B., Weinreb, S., 1999, IEEE Trans. Microwave Theory Tech., 47, 2212
Finkenzeller, U., Mundt, R., 1984, A&AS, 55, 109
Fuente, A., Martin-Pintado, J., Bachiller, R., Neri, R., Palla, F., 1998, A&A, 334, 253
Giard, M., Bernard, J.P., Lacombe, F., Normand, P., Rouan, D., 1994, A&A, 291, 239
Hatchell, J., Richer, J.S., Fuller, G.A., Qualtrough, C.J., Ladd, E.F., Chandler, C.J., 2005, A&A, 440, 151
Johnstone, D., Di Francesco, J., Kirk, H., 2004, ApJ, 611, L45
Kallas, E., Reich, W., 1980, A&AS, 42, 227
Kenyon, S.J, Hartmann, L., 1995, ApJS, 101, 117
Kerton, C.R., Ballantyne, D., Martin, P.G., 1999, AJ, 117, 2485
Kerton, C.R., Martin, P.G., Johnstone, D., Ballantyne, D.R., 2001, ApJ, 552, 601
Kirk, H., Johnstone, D., Di Francesco, J., 2006, ApJ, 646, 1009
Koornneef, J., A&A, 1983,128, 84
McKee, C., 1999, in Lada, C.J., Kylafis, N.D., eds, The Origin of Stars and Planetary Systems. Kluwer, Dordrecht, p. 29
Moore, T.J.T., Bretherton, D.E., Fujiyoshi, T., Ridge, N.A., Allsopp, J., Hoare, M.G., Lumsden, S.L., Richer, J.S., 2007, MNRAS, 379, 663
Neuhasuer, R., Frink, S., Torres, G., Sterzik, M.F., Roeser, S., Randich, S., 1998 in Donahue, R.A. Bookbinder, J.A., eds, ASP Conf. Ser. Vol. 154, The Tenth Cambridge Workshop on Cool Stars, Stellar Systems and the Sun. Astron. Soc. Pac., San Francisco, p. 1748
Onishi, T., Mizuno, A., Kawamura, A., Ogawa, H., Fukui, Y., 1998, ApJ, 502, 296
Osterbrock, D.E., 1985, Astrophysics of Gaseous Nebulae and Active Galactic Nuclei, University Science Books, Sausalito, CA
Price, S.D., Egan, M.P., Carey, S., Mizuno, D.R., Kuchar, T.A., 2001, AJ, 121, 2819
Rieke, G.H., Lebofsky, M.J., 1985, ApJ, 288, 618
Robitaille, T.P., Whitney, B.A., Indebetouw, R., Wood, K., Denzmore, P., 2006, ApJS, 167, 256
Roger, R.S., Dewdney, P.E., 1992, ApJ, 385, 536
Ruffle, D.P., Hartquist, T.W., Rawlings, J.M.C.,Williams, D.A., 1998, A&A, 334, 678
Rydgren, A.E., Vrba, F.J., 1983, AJ, 88, 1017
Skrutskie, M.F. et al., 2006, AJ, 131, 1163
Strong, A.W., Mattox, J.R., 1996, A&A, 308, 21
Thé, P.S., de Winter, D., Pérez, M.R., 1994, A&AS, 104, 315